Food & Function

ROYAL SOCIETY OF CHEMISTRY

PAPER

View Article Online
View Journal | View Issue

Cite this: *Food Funct.*, 2025, **16**, 2972

Malus hupehensis leaves: a functional beverage for alleviating hepatic inflammation and modulating gut microbiota in diabetic mice†

Qiue Zhang, ‡[a,b] Tong Su,‡[b,c] Yajing Pan,[d] Xiaomeng Wang,[b] Chengfei Zhang,[c] Huizhao Qin,[b,c] Mingxiu Li,[b,e] Qingsong Li,[b,f] Xiaochen Li,[a,b] Jiangfan Guo,[b,f] Lili Wu,[b] Lingling Qin[b] and Tonghua Liu*[b]

Malus hupehensis leaves (MHL), consumed as a daily beverage in Chinese folk tradition and recently recognized as a new food material, are abundant in polyphenols and bioactive compounds that demonstrate hypoglycemic, lipid-lowering, and anti-inflammatory effects. However, the antidiabetic mechanisms have not been fully elucidated. This study aimed to investigate the protective mechanisms of *Malus hupehensis* leaves' extract (MHLE) against type 2 diabetes mellitus (T2DM). The results showed that MHLE effectively ameliorated glucose and lipid metabolic abnormalities in db/db mice, and attenuated hepatic macrophage activation. Transcriptomic analysis of the liver revealed that MHLE primarily affects genes involved in inflammatory responses and inhibited the TLR4/MAPK pathway to reduce hepatic inflammation. Metagenomic sequencing identified changes in gut microbiota composition and showed that MHLE restored the abundance of *Lachnospiraceae bacterium*, *Oscillospiraceae bacterium*, and *Clostridia bacterium* while reducing the abundance of *Escherichia coli*, thereby ameliorating gut dysbiosis. The integrated regulation of metabolism, immune response, and the microbial environment by MHLE significantly alleviated symptoms of T2DM. This study offers strong scientific evidence for the potential use of MHL as a functional food.

Received 31st October 2024,
Accepted 26th February 2025

DOI: 10.1039/d4fo05325g

rsc.li/food-function

Introduction

The global prevalence of type 2 diabetes mellitus (T2DM) is escalating, posing an ongoing challenge to its prevention and control.[1,2] As a complex metabolic disorder, the exact pathogenesis of T2DM remains unclear, but it is generally believed to involve multiple factors including genetics, environmental exposures, insulin resistance, and pancreatic β-cell dysfunction.[3] In recent years, the interaction between the gut and the liver, known as the "gut–liver axis", has received increasing attention for its role in the pathogenesis of T2DM.[4] Diabetic patients often exhibit dysbiosis in their gut microbiota, characterized by a significant increase in pathogenic and opportunistic Gram-negative bacteria and a relative decrease in symbiotic bacteria.[4] Some Gram-negative bacteria, such as members of the genus Bacteroides, have been demonstrated to possess a high pro-inflammatory potential, and their proliferation has been associated with elevated levels of lipopolysaccharide (LPS). An increase in LPS can induce metabolic endotoxemia and chronic inflammation, particularly in the liver, where bacterial endotoxins, metabolites, and components from the gut can lead to dysfunction of lysosomes, endoplasmic reticulum, and mitochondria. This results in a shift of macrophages toward M1 polarization, which releases a variety of pro-inflammatory cytokines, including tumor necrosis factor-α (TNF-α) and interleukin-6 (IL-6). This further exacerbates steatosis and insulin resistance.[5] In light of these findings, the gut-liver axis represents a significant potential avenue for therapeutic intervention in the management of T2DM.

The absorption function of the intestines and microbiome are essential prerequisites for the operation of the enterichepatic axis. Consequently, they are more susceptible to disruption by oral drugs or food. In recent years, there has been a notable increase in the popularity of functional foods, which often contain biologically active ingredients that are believed to offer physiological health benefits. These benefits may

[a]*School of Traditional Chinese Medicine, Beijing University of Chinese Medicine, Beijing, 102488, China*
[b]*Key Laboratory of Health Cultivation of the Ministry of Education, Beijing University of Chinese Medicine, Beijing, 102488, China. E-mail: thliu@vip.163.com*
[c]*Dongfang Hospital of Beijing University of Chinese Medicine, Beijing, 100078, China*
[d]*Institute of Basic Theory for Chinese Medicine, China Academy of Chinese Medical Sciences, Beijing, 100700, China*
[e]*School of Clinical Medicine, Chengdu University of Traditional Chinese Medicine, Chengdu, 610075, China*
[f]*Shaanxi University of Chinese Medicine, Xianyang, 712046, China*
†Electronic supplementary information (ESI) available. See DOI: https://doi.org/10.1039/d4fo05325g
‡These authors contributed equally to this study.

include enhanced antioxidant, anti-inflammatory, and lipid-lowering functions, particularly in the context of chronic metabolic diseases such as T2DM.[6] Some studies have demonstrated that functional foods comprising high-fiber, polyphenol-rich plant proteins such as erythrina and chia seeds can mitigate metabolic endotoxemia and enhance glycemic control, lipid metabolism, and chronic inflammatory responses in individuals with T2DM by modulating the fecal microbiome.[7] Some herbal plants rich in polyphenols, including coffee, green tea, black tea, and mate, have been demonstrated to confer clinically significant benefits in the context of glucose and lipid metabolism, anti-inflammatory activity, and antioxidant function in patients with T2DM.[6]

Malus hupehensis (Pamp.) Rehd., a member of the Rosaceae family, is widely distributed in southern China. The young leaves of this plant, also known as "tea crabapple", are commonly consumed as tea in Chinese folk cultureand have been classified as a new food material by the National Health Commission of China.[8] Pharmacological studies indicated[8] that these leaves are rich in polyphenols, proteins, and various essential trace elements, and exhibit multiple biological activities, including hypoglycemic and lipid-lowering effects. Although the hypoglycemic effect of *Malus hupehensis* leaves (MHL) has been preliminarily confirmed,[9] the underlying mechanisms have not been fully elucidated. This study used C57BLKS/J-db/db (db/db) mice, a spontaneous animal model of T2DM, to evaluate the hypoglycemic efficacy and safety of *Malus hupehensis* leaves' extract (MHLE). In addition, potential mechanisms were explored using transcriptomics and metagenomics multi-omics analyses to unlock the potential of MHL as a functional food. The findings of this study indicate that MHL has the potential to serve as a promising dietary intervention for the management of T2DM and that it provides scientific support for its development as a functional food.

Materials and methods

Preparation and quality control of MHLE

MHL was purchased from Wuhan Meiren Yifen Trading Co., Ltd (Wuhan, China). MHL is commonly used as a kind of tea to be brewed and consumed. In order to better simulate its drinking experience, we adopted a water extraction method. The leaves were extracted twice with boiling water, and the resulting solution was concentrated under reduced pressure using a rotary evaporator. The concentrated extract was first frozen and then dried in a freeze dryer at −80 °C under vacuum for more than 12 hours. After drying, MHLE was aliquoted, sealed, and stored at −20 °C. Referring to the previous method,[10] the ultra high performance liquid chromatography coupled with quadrupole electrostatic field orbitrap mass spectrometry (UHPLC-QE-MS) technique is adopted to detect the components of MHLE. Phloretin and other compounds were quantitatively analyzed using high-performance liquid chromatography. Accurately weigh 52 mg of the aforementioned MHLE, add 1 mL of 80% methanol solution, and perform ultrasonic extraction for 1 hour. Collect 100 μL of the supernatant, then prepare serial dilutions at factors of 2, 10, 100, and 1000 for mass spectrometry analysis. Chromatographic separation was performed on a Waters ACQUITY UPLC I-CLASS system equipped with a Waters UPLC HSS T3 column (2.1 × 100 mm, 1.8 μm) using a gradient mobile phase: (A) acetonitrile–water (1 : 10, 0.04% acetic acid, 1 mM ammonium acetate) and (B) acetonitrile–isopropanol (1 : 1). The gradient elution program was set as follows: 0–1.5 min (99% A), 1.5–13 min (99% → 60% A), 13–14 min (60% → 0% A), 14–18 min (100% B), and 18.1–20 min (re-equilibration to 99% A), with a flow rate of 0.3 mL min^{-1}, injection volume of 3.0 μL, and column temperature at 45 °C. Mass spectrometry analysis was conducted on a Waters XEVO TQ-S Micro triple quadrupole system in both ESI^+ and ESI^- modes. Key parameters included ion source voltage (1.6 kV), desolvation temperatures (450 °C for ESI^+, 500 °C for ESI^-), desolvation gas flow rates (800 L h^{-1} for ESI^+, 1000 L h^{-1} for ESI^-), and cone gas flow (10 L h^{-1}). Data were processed using TargetLynx software with quantification based on standard curves (reference standards: phloretin, phlorizin, kaempferol-3-*O*-rutinoside, baicalin, myricitrin, chlorogenic acid, chrysin, *p*-hydroxy-cinnamic acid, rutin, naringenin, and ursolic acid; sourced from Manste Biotech Co., Ltd, Chengdu, China).

Animals and experimental protocols

Five-week-old male db/db mice and C57BL/KSJ-wt/wt (wt/wt) mice were purchased from GemPharmatech Laboratory (#E2309250648, Nanjing, China). All animal experimental procedures were conducted in accordance with the National Institutes of Health Guide for the Care and Use of Laboratory Animals and were approved by the Animal Care and Ethics Committee of Beijing University of Traditional Chinese Medicine (No.: BUCM-2023091906-3197). Mice were housed in a barrier environment at Beijing University of Traditional Chinese Medicine, with controlled temperature (20–26 °C) and humidity (40–70%) under a 12-hour light/dark cycle. All mice had free access to normal chow diet and water.

Following a one-week period of adaptive feeding, the mice were fasted for a period of six hours, during which time they had free access to water. Subsequently, a blood glucose measurement was taken *via* the tail vein using a Contour Plus Blood Glucose Meter (85271938, Bayer, Germany). The designation of diabetic mice was based on the criterion of fasting blood glucose (FBG) levels exceeding 11.1 mmol L^{-1}.[11] A total of 35 diabetic mice were selected and randomly divided into five groups. The diabetes mellitus group (DM group) received double-distilled water, the metformin group (MET group) received 200 mg kg^{-1} d^{-1} metformin[12]. The MHLE-H, MHLE-M, and MHLE-L groups received MHLE at doses of 700 mg kg^{-1} d^{-1}, 350 mg kg^{-1} d^{-1}, and 175 mg kg^{-1} d^{-1}, respectively. These doses were calculated based on the human-mouse body surface area conversion formula,[13] corresponding to human equivalent doses of 30 g d^{-1}, 15 g d^{-1}, and 7.5 g d^{-1} crude MHL, which requires brewing with hot water. According to guidelines from China's National Health Commission, the

recommended maximum daily dose is 15 g. Consequently, we established three gradient doses aligned with this guidance. As reported in previous literature,[14] these doses correspond to total flavonoid contents in crude MHL of 589.5–629.1 mg d^{-1}, 294.75–314.55 mg d^{-1}, and 147.375–157.275 mg d^{-1}, respectively. For adults, these dosages fall within the typical daily dietary intake range of total flavonoids.[15] All vehicles used for compound delivery were double distilled water. The wt/wt mice (normal control group, NC group) received an equal volume of double distilled water. All mice were gavaged once daily.

The experiment lasted five weeks with weekly monitoring of body weight, fasting blood glucose, food and water consumption. After four weeks of treatment, an oral glucose tolerance test (OGTT) was performed by orally administering a glucose solution (1 g kg^{-1}) to db/db and wt/wt mice. Blood glucose levels were measured at 0, 30, 60, 90, and 120 min after glucose administration, and the area under the curve (AUC) was calculated. After five weeks of treatment, all mice were fasted for 12 hours with free access to water. Blood samples were collected from the retro-orbital venous plexus under deep anesthesia, and serum was separated by centrifugation. Liver, colon and other tissues were collected for fixation or freezing. The left epididymal fat pad and liver were weighed, and the liver index was calculated using the following formula: liver index = liver weight (g)/body weight (g) × 100%. The body length of the mice (distance from the tip of the nose to the anus) was measured, and the Lee's index was calculated as Lee's index = body weight (g)^(1/3) × 10/body length (mm).

Plasma biochemistry analysis

Serum was obtained from the centrifuged blood samples as described above. Serum levels of alanine aminotransferase (ALT), aspartate aminotransferase (AST), triglycerides (TG), total cholesterol (TC), low-density lipoprotein (LDL), high-density lipoprotein (HDL), creatinine (CREA), and blood urea nitrogen (UREA) were measured using a BS-420 automatic biochemical analyzer (Mindray Bio-Medical, China). Additionally, glycated serum protein (GSP) (HY-N0037, Huaying Biotechnology, China), and LPS (HEB526Ge, CLOUD-CLONE CORP, China) were measured according to the manufacturers' instructions.

Histological observation

Fresh liver and colon tissues were fixed in 4% paraformaldehyde solution and embedded in paraffin and prepared into sections 4 μm thick. Hematoxylin and eosin (HE) staining was performed for morphological observation, while Periodic Acid-Schiff (PAS) staining was used to detect glycogen content in the liver. In addition, liver also embedded in opti-mum cutting temperature compound to make frozen sections for Oil Red O staining to detect lipid accumulation.

Immunohistochemistry staining

The paraffin-embedded colon tissue sections were deparaffinized, hydrated, and subjected to antigen retrieval. The sections were permeabilized with 0.01% Triton X-100, peroxidase was blocked with 3% hydrogen peroxide, and the sections were blocked with goat serum. The sections were incubated at 4 °C overnight with primary antibodies against Zonula Occludens-1 (ZO-1) (21773-1-AP, Proteintech, 1 : 200) and Occludin (66378-1-Ig, Proteintech, 1 : 200). On the subsequent day, the sections were labeled with the secondary antibody, visualized with DAB, and counterstained with hematoxylin. Subsequently, the differentiation, dehydration, and mounting of the sections were conducted, after which they were observed under a microscope.

Immunofluorescence staining

The liver sections that had been embedded in paraffin were subjected to a series of processes, commencing with de-paraffinization and continuing with hydration, permeabilization with 0.1% Triton X-100, and peroxidase blocking with 3% hydrogen peroxide. Subsequently, the sections were blocked with goat serum and incubated overnight at 4 °C with primary antibodies. The antibodies were sourced from Cell Signaling. The following antibodies were used: F4/80 (30325, 1 : 2000), CD86 (19589, 1 : 2000), CD206 (24595, 1 : 3000). On the subsequent day, the sections were labeled with fluorescent secondary antibodies, counterstained with 4′,6-diamidino-2-phenylindole (DAPI), and observed under a fluorescence microscope.

Transcriptome analysis

Liver tissues from four randomly selected mice from each group were used for RNA extraction. The concentration and purity of the RNA were detected by Nanodrop2000, and the integrity of RNA was detected by agarose gel electrophoresis. Then magnetic beads with Oligo(dT) were used to pair A–T bases with ployA at the 3′ end of mRNA. The mRNA was then fragmented and reverse transcribed into cDNA. Adapter sequences were added to the cDNA ends, and the purified and size-selected cDNA was used to construct a sequencing library. High-throughput sequencing was performed on the NovaSeq X Plus platform (PE150, Illumina, USA). DESeq2 is used to screen for differential genes, bioinformatics analysis was conducted using the online tools of the Majorbio Cloud Platform (**https://cloud.majorbio.com/page/tools/**).

Metagenomes analysis

Metagenomic sequencing of the gut microbiota was conducted as previously described.[16] Colonic contents from four randomly selected mice from each group were used for genomic DNA extraction, followed by concentration, purity, and integrity assessment. Sample DNA extraction was performed according to the instructions of the PF Mag-Bind Stool DNA Kit (Omega Bio-tek, USA), and DNA integrity was tested using 1% agarose gel electrophoresis. PE libraries were then constructed by DNA fragmentation using Covaris M220 (Genomics, China) and the products were screened and recovered using magnetic beads, which were amplified by bridge PCR and then metagenomic sequencing was performed using Illumina NovaSeq (Illumina, USA) sequencing platform. After data quality

control, the sequencing results were compared with multiple databases to obtain species taxonomy and functional annotations, and the differences of species and functions among groups were analyzed. The Kruskal–Wallis H test was employed for the comparison of multiple groups, and the results were calibrated using the BH method for multiple tests. Furthermore, a Spearman correlation analysis was employed to examine the relationship between species-level flora and serum LPS, hepatic TNF-α, IL-6, and C–X–C motif chemokine ligand 1 (*Cxcl1*). These analyses were conducted using the online tools of the Majorbio Cloud Platform (**https://cloud.majorbio.com/page/tools/**).

Quantitative real-time polymerase chain reaction (RT-qPCR)

Using the RNA Easy Fast Tissue/Cell Kit (DP451, TIANGEN, China), total RNA was extracted from liver tissues. Subsequently, RNA was reverse transcribed into cDNA using the ABScript Neo RT Master Mix for QPCR (RK20433, Abclonal, China). The cDNA was amplified using the BrightCycle Universal SYBR Green QPCR Mix (RK21219, ABclonal, China). Primers were purchased from Sangon Biotech (China), and the sequences are listed in ESI Table S1.† The relative expressions of the target genes were determined by the $2^{-\Delta\Delta Ct}$ method using *Actb* as the control.

Western blot

The liver tissues were weighed and an appropriate amount was collected for protein extraction. After protein quantification and denaturation, the samples were separated using a 10% SDS-PAGE gel electrophoresis system and transferred to a polyvinylidene fluoride membrane. The membrane was blocked for 1 hour at room temperature and then incubated with primary antibodies for 12 hours at 4 °C. Primary antibodies against p38 (8690), p-p38 (4511), JNK (67096), p-JNK (4668), ERK (4695), p-ERK (3192), TLR4 (14358), and β-actin (4970) were purchased from Cell Signaling Technology and used at 1 : 1000 dilution. The membrane was then incubated with a 1 : 10 000 dilution of secondary antibody (ab205718, Abcam, USA) for 1 hour at room temperature. Images were captured using the Universal Hood Imaging System (Bio-rad, USA) after incubation with ECL substrate, and protein quantification was performed using Image J software (NIH, USA).

Multiplex analysis of liver cytokines

Electrochemiluminescence was used to detect changes in inflammatory cytokines and chemokines in liver tissues. An appropriate amount of liver tissue was weighed, and 200–300 μL of lysis buffer was added per 10 mg of tissue. The tissues were homogenized using a tissue grinder and incubated at 4 °C for 20 minutes. The mixture was then centrifuged at 13 000 rpm for 10 minutes at 4 °C, and the supernatant was collected and quantified. According to the manufacturer's instructions for the V-PLEX kit (MSD, K15048D, USA), samples were loaded, incubated, and washed. Detection was performed using the MSD SQ120 system (Meso Scale Discovery, USA), and data analysis was conducted with DISCOVERY WORKBENCH software (Version 4.0, Meso Scale Discovery, USA).

Statistical analysis

Statistical analysis was performed using SPSS 25.0 software (IBM, USA). Data that conformed to a normal distribution were expressed as mean ± standard deviation (mean ± SD). Multiple group comparisons were conducted using one-way analysis of variance, followed by Fisher's least significant difference (LSD) test when homogeneity of variances was satisfied, or Dunnett's T3 Post-Hoc test when variances were not homogeneous. Data that did not conform to a normal distribution were expressed as median (quartile 25%, 75%) [M (Q1, Q3)] and compared using the Kruskal–Wallis one-way analysis of variance by ranks test. A value of $P < 0.05$ was considered statistically significant.

Results

Identification of MHLE compounds

To ensure consistency and quality of components, a UHPLC-QE-MS-based non-targeted metabolomics approach was utilized to investigate differences in precursor metabolite components in MHLE. The base peak plot is shown in Fig. 1. The data were compared with databases. A total of 21 103 valid compounds were detected, with 2657 annotated compounds (details are provided in the ESI†) and 18 446 unknown compounds. Among the annotated compounds, 156 were classified as Level 1(full match of primary mass spectrum, secondary mass spectrum and retention time with an authentic chemical standard under identical experimental conditions), 548 as Level 2 (full match of primary mass spectrum and secondary mass spectrum with public database entries), and 1953 as Level 3 (chemical class assignment based on class-specific physicochemical features or theoretical spectral predictions).[17] The identified compounds were primarily flavonoids, triterpenoids, and phenolic acids. These compounds were matched with those reported in previously published articles.[8,18–20] The quantitative analysis of twelve compounds revealed the following contents: in the flavonoid group, the following compounds were quantified: phlorizin (147.80 mg g^{-1}), quercetin-3-*O*-glucoside (2.77 mg g^{-1}), phloretin (0.45 mg g^{-1}), rutin (48.49 μg g^{-1}), naringenin (8.02 μg g^{-1}), myricitrin (6.47 μg g^{-1}), kaempferol-3-*O*-rutinoside (3.46 μg g^{-1}), chrysin (0.30 μg g^{-1}), and baicalin (0.11 μg g^{-1}). The triterpenoid compound identified was ursolic acid (41.61 μg g^{-1}). Phenolic acids included chlorogenic acid (1.95 mg g^{-1}) and *p*-hydroxy-cinnamic acid (0.10 mg g^{-1}). Phlorizin had the highest content, followed by quercetin-3-*O*-glucoside and chlorogenic acid.

Effects of MHLE on glucose and lipid metabolism profile in db/db mice

As shown in Fig. 2A, the animal component of the study was conducted with strict adherence to the established experimental design. Turning to Fig. 2B, from the first to the fifth week of the experiment, a decreasing trend in FBG levels was

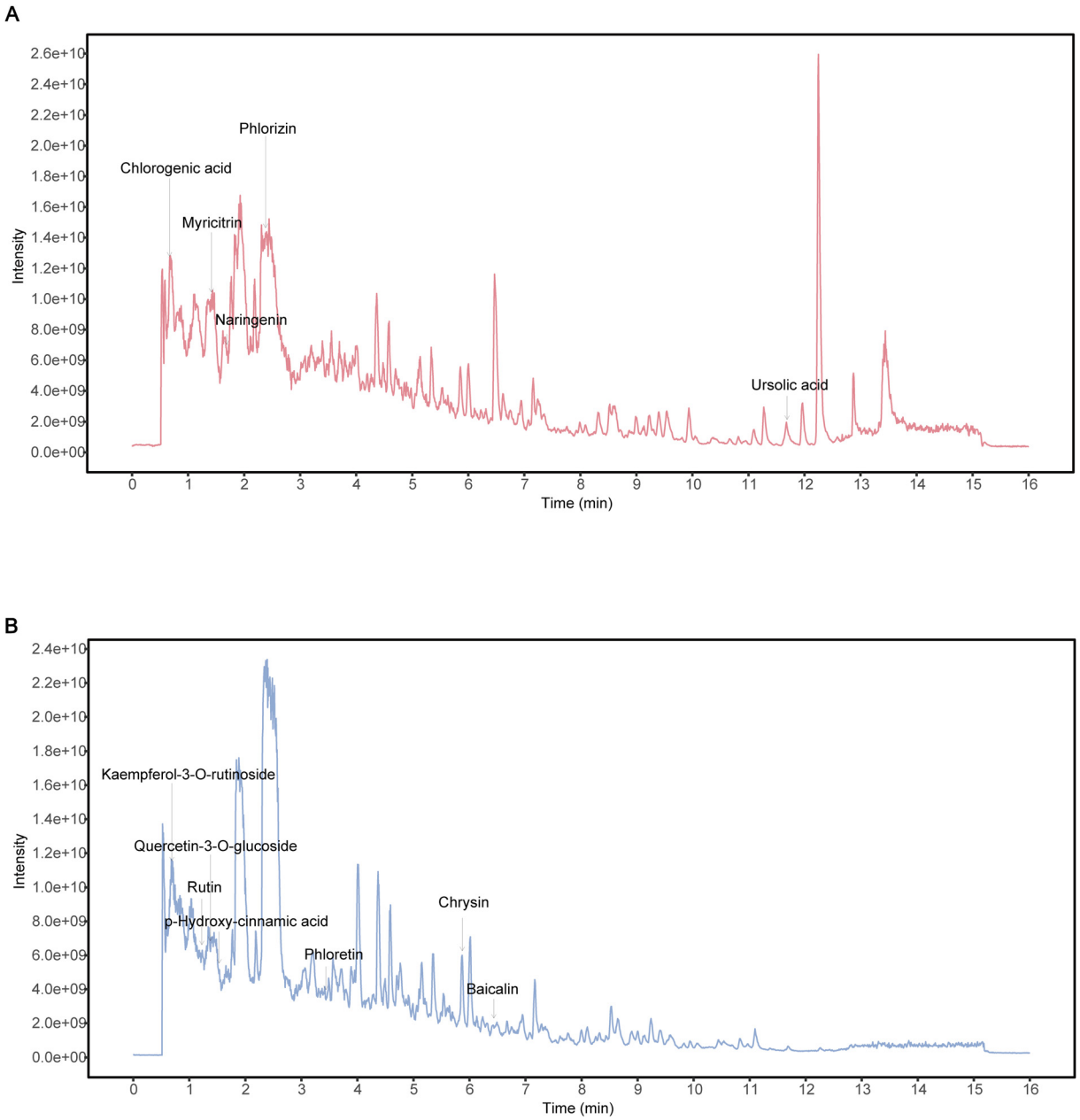

Fig. 1 Mass Spectra of MHLE. (A) Base peak chromatogram in positive ion mode. (B) Base peak chromatogram in negative ion mode.

observed in all MHLE dosing groups, in contrast to the DM group. After five weeks of medical intervention, a significant alleviation of elevated fasting glucose levels was observed in the MHLE-H (Dunnett's T3 test, P = 0.001), MHLE-M (Dunnett's T3 test, P = 0.011), and MHLE-L (Dunnett's T3 test, P < 0.001) groups compared to the DM group. In addition, MHLE significantly improved glucose tolerance in db/db mice, with the MHLE-L group showing the most pronounced decrease in AUC among the treated groups (Fig. 2C and D). GSP levels decreased in all MHLE dose groups (Dunnett's T3 test, P < 0.05) (Fig. 2E), further supporting the positive influence of MHLE on blood glucose regulation throughout the experimental period. By systematically monitoring food intake and water consumption (Fig. 2F and G), we observed a trend indicating the ability of MHLE to alleviate the symptoms of polydipsia and polyphagia in diabetic mice. After five weeks of drug intervention, no statistically significant differences in body weight were observed between the MHLE groups and the DM group (Dunnett's T3 test, P > 0.05), nor was there a statistical difference in Lee's index (LSD test, P > 0.05) (Fig. 2H and I). This indicates that MHLE has a limited effect on body weight and fat distribution in the short term. However, we observed a decrease in epididymal fat mass in the MHLE-H (Dunnett's T3 test, P = 0.044) and MHLE-L (Dunnett's T3 test, P = 0. 046)

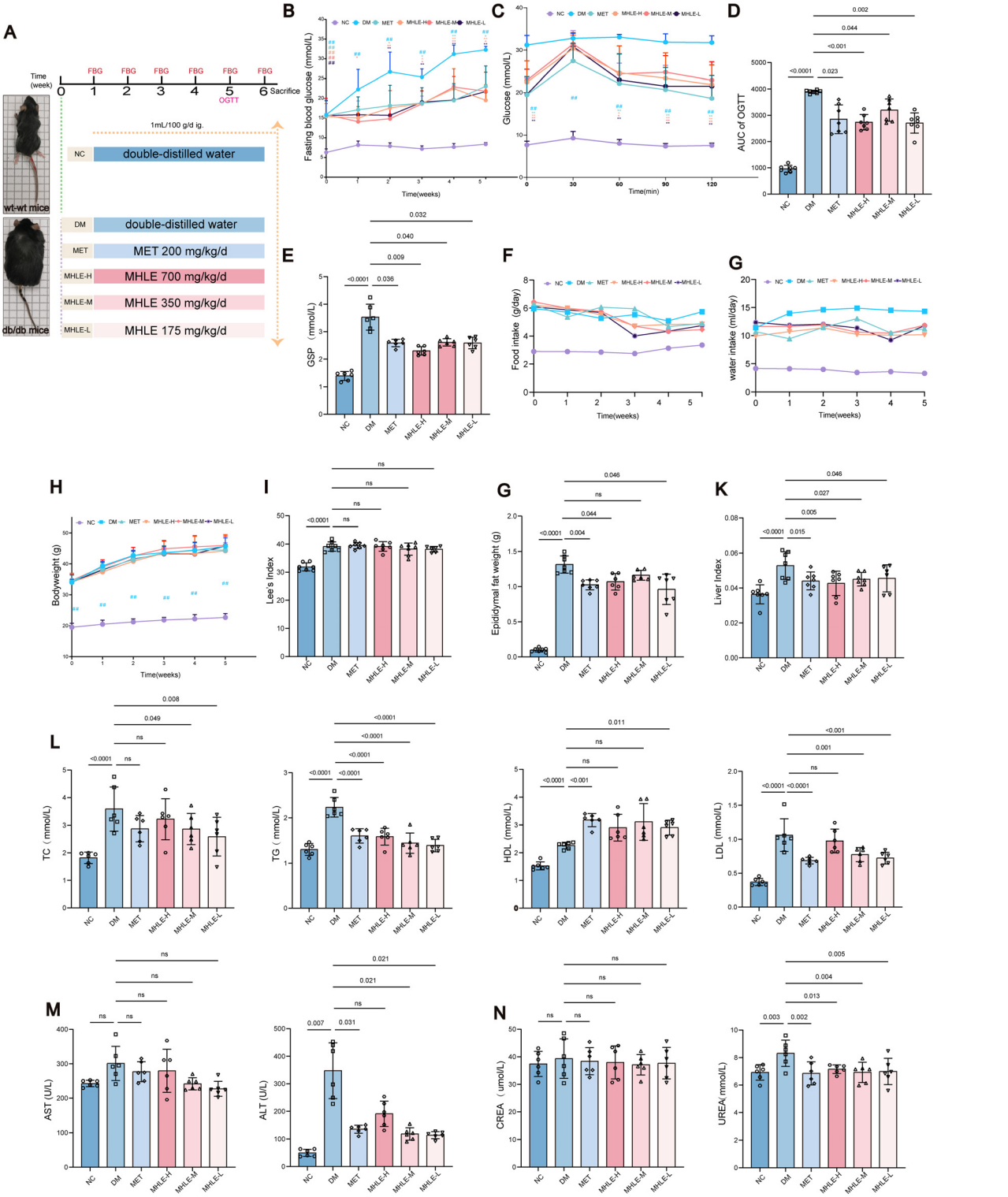

Fig. 2 MHLE improves glucose and lipid metabolism profiles in db/db mice. (A) Experimental design for MHLE treatment in diabetic mice. (B) Dynamic curve of fasting blood glucose. (C and D) OGTT and AUC. (E) Changes in GSP. (F and G) Food and water intake. (H) Dynamic curve of body weight. (I–K) Differences in obesity indicators: Lee's index, epididymal fat weight, liver index. (L) Changes in blood lipids. (M and N) Liver and kidney function. (n = 6–7 biological replicates, mean ± SD, # $P < 0.05$, ## $P < 0.01$ *vs.* the NC group, *$P < 0.05$, **$P < 0.01$ *vs.* the DM group. ns $P > 0.05$).

groups compared to the DM group, and a decrease in liver tissue index was observed in all three MHLE dose intervention groups with statistically significant differences (LSD test, $P < 0.05$) (Fig. 2G and K), reflecting the beneficial role of MHLE in ameliorating visceral fat accumulation and promoting liver health.

Regarding the regulation of lipid profiles (Fig. 2L), in contrast to the diabetic model group (DM group), all dosage groups significantly reduced TG levels (LSD test, $P < 0.05$). Specifically, the low-dose group (MHLE-L) not only significantly reduced TC levels (LSD test, $P = 0.008$), but also significantly increased HDL levels (Dunnett's T3 test, $P = 0.011$). In addition, LDL levels were significantly reduced in both the MHLE-M and the MHLE-L group (LSD test, MHLE-M: $P = 0.001$; MHLE-L, $P < 0.001$).

Effects of MHLE on liver and kidney function in db/db mice

When evaluating liver and kidney function (Fig. 2M and N), the MHLE-M and MHLE-L groups demonstrated a notable decline in ALT levels when compared to the DM group (Dunnett's T3 test, $P < 0.05$). Concurrently, UREA levels exhibited a significant reduction across all MHLE dose groups in comparison to the DM group (LSD test, $P < 0.05$). AST and CREA levels showed no significant differences between the groups, likely due to their slower changes. ALT is mainly found in the hepatocyte cytoplasm, while AST is primarily located in mitochondria and is only released into the blood when liver cells are severely damaged.[21] Moreover, AST is present in other tissues such as the heart, muscles, and kidneys, meaning its elevation does not exclusively reflect liver damage.[22] In contrast, ALT is more liver-specific. CREA is a marker of kidney filtration, but its levels typically rise only with significant kidney damage.[23] The increased ALT and UREA levels in the model group indicate hepatic and renal damage in db/db mice, with MHLE helping to delay the progression of these impairments.

Effects of MHLE on pathological morphology of liver in db/db mice

The liver is a vital organ centrally involved in the biosynthesis of lipids, the generation of glucose, and the metabolism of cholesterol.[24] The histologic staining results for the liver are shown in Fig. 3. After HE staining and microscopic examin-

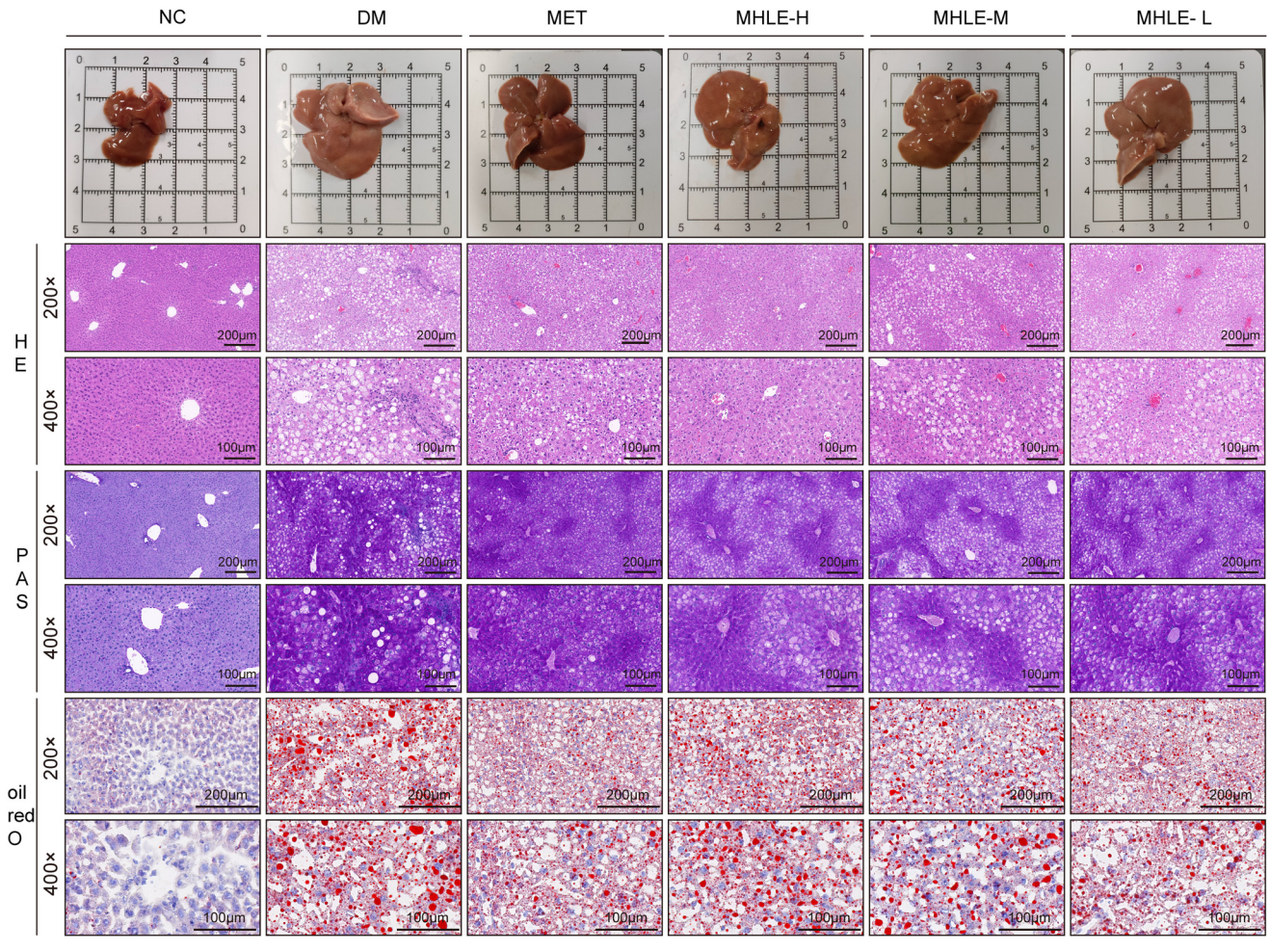

Fig. 3 Liver morphology and histopathological staining. Representative images of mice liver using HE, PAS, and oil red O staining at 200× magnification (scale bars: 200 μm) and 400× magnification (scale bars: 100 μm).

ation, liver cells in the NC group were observed to radiate around the central vein, with normal morphology, large and round centrally located nuclei, and homogeneous cytoplasm without fatty degeneration. Cells in the DM group showed disorganized arrangement, severe fatty degeneration, and diffusely distributed inflammatory cells. In contrast to the DM group, less fatty degeneration, more regular arrangement, and less inflammatory infiltration were observed in the liver cells of the MET group and those treated with low, medium, and high doses of MHLE. PAS staining results showed that the NC group had fewer purple-red granules with a lighter hue, indicating that wt/wt mice had less glycogen storage in the liver after a 12-hour fast. The DM group had an abundance of purple-red granules with a deeper shade, indicating that hyperglycemia led to excessive accumulation of glycogen, a condition that was ameliorated by MHLE treatment. Oil red O staining showed fewer stained lipid droplets in the liver tissue of NC group mice. Lipid droplets in liver cells of DM group mice were red, diffusely and granularly accumulated, and coalesced into spots. Compared with the DM group, a significant reduction in the number of lipid droplets was observed in the liver cells of mice in all treated groups, and the size of the lipid droplets was relatively smaller.

Effects of MHLE on hepatic macrophages in db/db mice

Analysis of glucose and lipid metabolism and histopathological results indicated that low-dose MHLE achieved the best effect, stabilizing blood glucose levels with minimal variation within the group and showing superior improvement in lipid levels. To further explore the underlying mechanisms, we selected the MHLE-L group for subsequent research, the MHLE group is specifically referred to as the MHLE-L group in the following results.

As mentioned above, we observed in liver histology that MHLE ameliorated inflammatory infiltration within the liver tissue. Therefore, we further examined the expression of surface markers on macrophages in the liver of mice from each group using immunofluorescence techniques (Fig. 4A

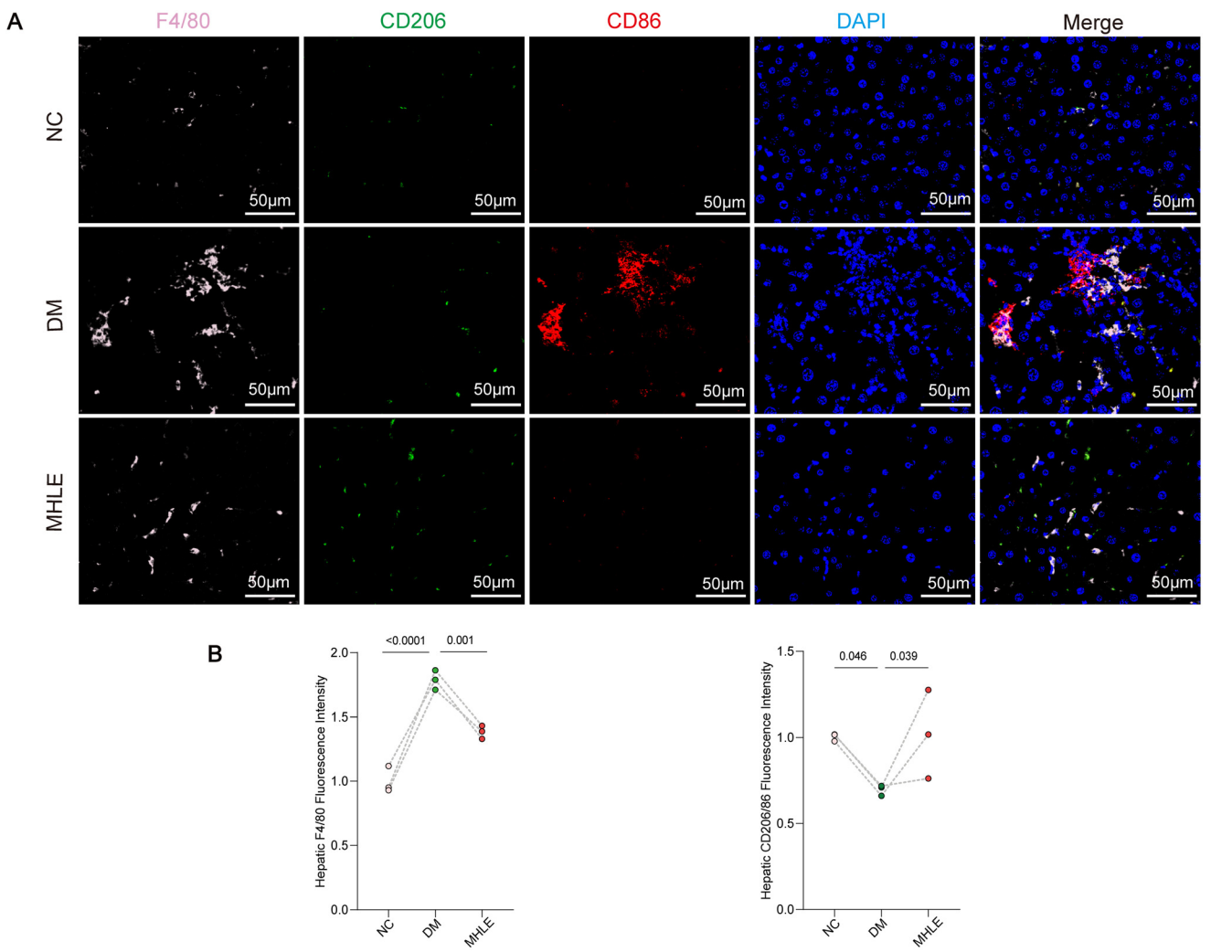

Fig. 4 MHLE inhibits macrophage activation. (A) Immunofluorescence of liver sections using anti-F4/80, anti-CD208, or anti-CD86 antibodies at 400× magnification (scale bars: 50 μm, n = 3 biological replicates). (B) Quantitative fluorescence analysis.

and B). Among these markers, F4/80 is primarily used to localize macrophages, CD208 is a marker for M2 macrophages, and CD86 is a marker for M1 cells. Therefore, the ratio of CD206/CD86 indicates the ratio of M2 to M1 macrophages. Compared with the NC group, the DM group showed a significant increase in the total number of macrophages (LSD test, $P < 0.001$) along with a decrease in the CD206/CD86 ratio (LSD test, $P = 0.046$), suggesting that diabetes-associated pathological changes are primarily characterized by an increase in M1 macrophages. In contrast to the DM group, the MHLE group showed a smaller increase in total macrophage count (LSD test, $P = 0.001$), accompanied by a significant recovery of the CD206/CD86 ratio (LSD test, $P = 0.039$).

Effects of MHLE on the hepatic transcriptome in db/db mice

To perform a comprehensive analysis of how MHLE affects hepatic gene expression, we used transcriptomics to detect changes in gene expression following MHLE treatment. Using thresholds of $P < 0.05$, fold change ≥ 1.5, or fold change ≤ 0.66, our results showed that the DM group had 2127 upregulated and 1402 downregulated genes compared to the NC group; conversely, the MHLE group had 358 upregulated and 765 downregulated genes compared to the DM group (Fig. 5A). The principal component analysis (PCA) plot showed a clear separation between the groups (Fig. 5B). In the gene ontology (GO) based transcriptomic analysis (Fig. 5C), the enriched pathways reflected critical biological processes associated with immune response, metabolic regulation, and inflammatory response within the samples. Kyoto encyclopedia of genes and genomes (KEGG) enrichment analysis revealed that the differentially expressed genes in the DM and MHLE groups were predominantly associated with the Toll-like receptor, TNF, and MAPK pathways (Fig. 5D). The heat map specifically depicted the genes enriched in these pathways (Fig. 5E).

Effects of MHLE on the hepatic TLR4/MAPK pathway

To substantiate the reliability of the transcriptomic analys is results, we used qPCR to assess the expression of genes associated with the upstream and downstream of the TLR4/MAPK pathway in the liver tissue of mice from each group, including cluster of differentiation 14 (*Cd14*), cluster of differentiation 40 (*Cd40*), TLR4, mitogen-activated protein kinase kinase kinase 8 (*Map3k8*), mitogen-activated protein kinase kinase kinase 1 (*Map3k1*), C–C motif chemokine ligand 3 (*Ccl3*), C–C motif chemokine ligand 4 (*Ccl4*), *Cxcl1*, C–X–C motif chemokine ligand 2 (*Cxcl2*), *Tnf* (Fig. 6A). The results indicated that the expression of these genes was significantly lower in the liver of db/db mice after MHLE intervention compared to the DM group, with statistically significant differences.

Fig. 6B shows the expression of proteins related to the TLR4/MAPK pathway in the liver of mice from each group. The TLR4 expression level in the MHLE group was lower than that in the DM group (LSD test, $P = 0.016$). Further calculation of the ratio of phosphorylated target protein to total target protein revealed that p-p38MAPK/p38MAPK (LSD test, $P = 0.048$), p-JNK/JNK (LSD test, $P = 0.015$), and p-ERK/ERK (LSD test, $P = 0.011$) were all decreased compared with the DM group, indicating that the phosphorylation of these proteins was relatively decreased in the liver of mice after MHLE intervention.

The results of the detection of hepatic inflammatory factors and chemokines (Fig. 6C) showed that the levels of IL-6 (LSD test, $P < 0.001$), TNFα (Dunnett's T3 test, $P = 0.041$), and CXCL1 (Dunnett's T3 test, $P = 0.020$) were significantly decreased in the MHLE group, with statistically significant differences.

Effects of MHLE on colon and gut microbiota in db/db mice

In our research, the results of HE staining of the colon (Fig. 7A) showed that the NC group had normal and intact overall tissue structure, with abundant goblet cells visible in the mucosal lamina propria and closely arranged crypt structures. In contrast, the DM group showed localized necrosis and disappearance of crypt structures in the lamina propria, accompanied by interstitial fibrosis and inflammatory cell infiltration. Compared with the DM group, the MHLE group showed slight abnormalities in the overall structure of the colonic tissue, characterized by localized atrophy of a small number of goblet cells in the mucosal lamina propria and no apparent infiltration of inflammatory cells in the tissue interstitium.

To evaluate the integrity of the colonic barrier in mice from each group, we used immunohistochemistry to detect the expression of ZO-1 and Occludin proteins (Fig. 7B and C). Under light microscopy, we observed that the colonic structure in the NC group was intact with clear morphology, while ZO-1 and Occludin proteins were stained brownish-yellow with relatively deep staining. In contrast, goblet cells in the colon of the DM group were markedly atrophic with lighter brownish-yellow staining. The MHLE group showed deeper staining compared to the DM group, indicating increased expression of ZO-1 (LSD test, $P = 0.004$) and Occludin (LSD test, $P = 0.002$) proteins. The serum LPS level (Dunnett's T3 test, $P = 0.007$) was found to be decreased (Fig. 7D).

Subsequently, we analyzed the fecal microbiota of the mice colon by high-throughput metagenomic sequencing. To understand the extent of community differences between samples, we used principal coordinate analysis (PCoA) based on Bray-Curtis distance to assess the beta diversity index (Fig. 8A). We found that the microbial communities of the MHLE group were closer to those of the NC group and showed higher similarity compared to the DM group (ANOSIM, $R = 0.581$, $P = 0.005$), suggesting that MHLE modulates intestinal microbial diversity. At the phylum level (Fig. 8B), both MHLE and NC groups showed a high abundance of *Bacillota*, whereas the DM group was dominated by *Bacteroidota* and *Pseudomonadota*. At the species level (Fig. 8C), MHLE treatment significantly reduced the abundance of harmful bacteria such as *Escherichia coli*, while increasing the abundance of beneficial bacteria such as *Lachnospiraceae bacterium*. The Kruskal–Wallis H test shown in Fig. 8D further calculated the significant differences between groups at the species level. We used LDA effect size (LEfSe) analysis to further dissect the taxa responsible for differences between groups from the phylum

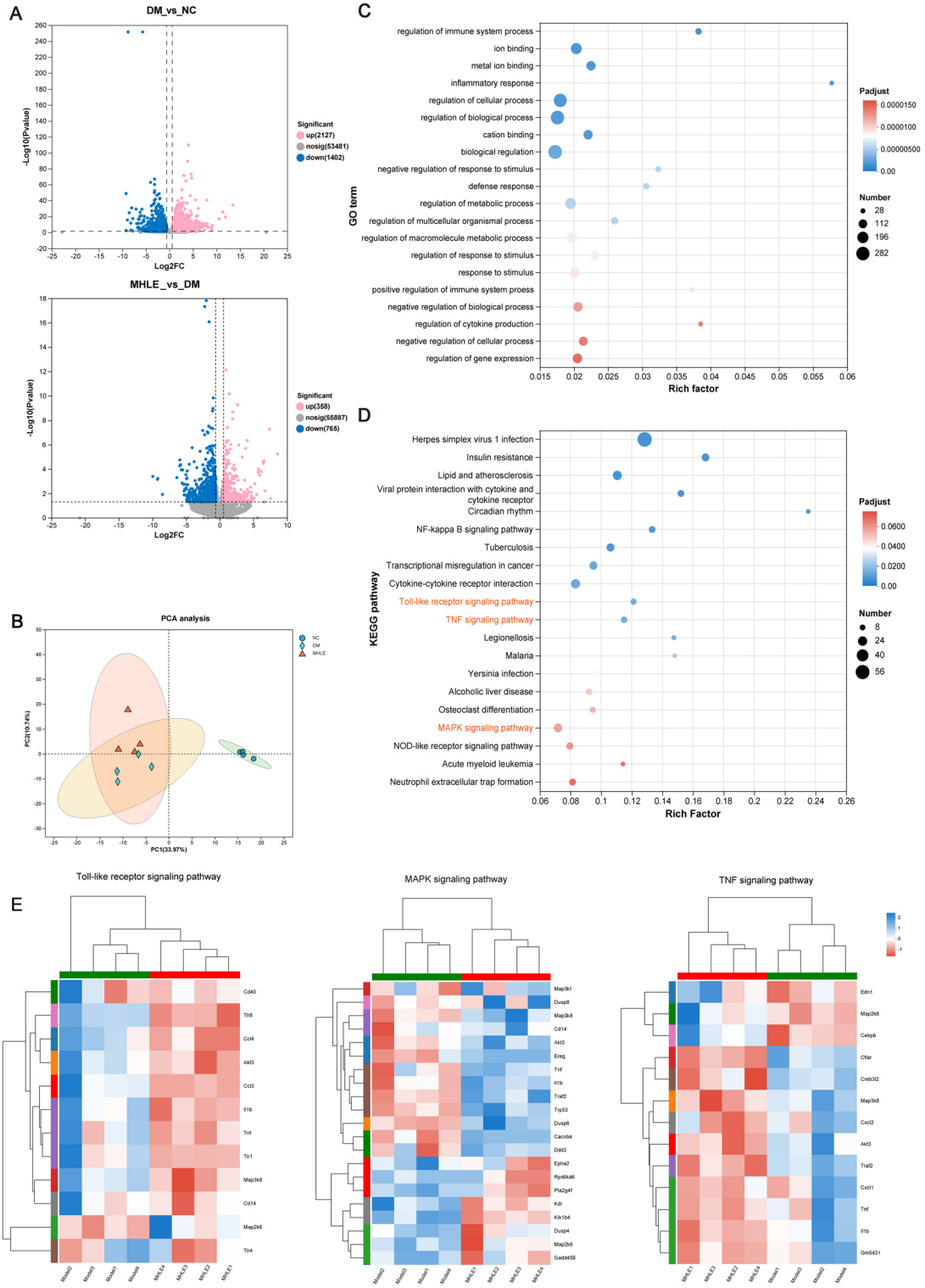

Fig. 5 Effects of MHLE intervention on hepatic differentially expressed genes (DEGs) in mice. (A) Volcano plot of DEGs between different groups (n = 4 biological replicates). (B) PCA analysis of the transcriptome. (C) GO terms between the MHLE and DM group. (D) KEGG terms between the MHLE and DM group. (E) Heatmap of enriched targets in the Toll-like receptor signaling pathway, MAPK signaling pathway, and TNF signaling pathway.

to the species level (Fig. 8E). The abundances of taxa at different levels vary across different groups. The figure shows key biomarkers in each group (LDA > 3.5, $P < 0.05$).

In addition to the analysis of gut microbiota composition, microbial functional annotation was performed using the KEGG database. The top 15 enriched pathways (level3) are

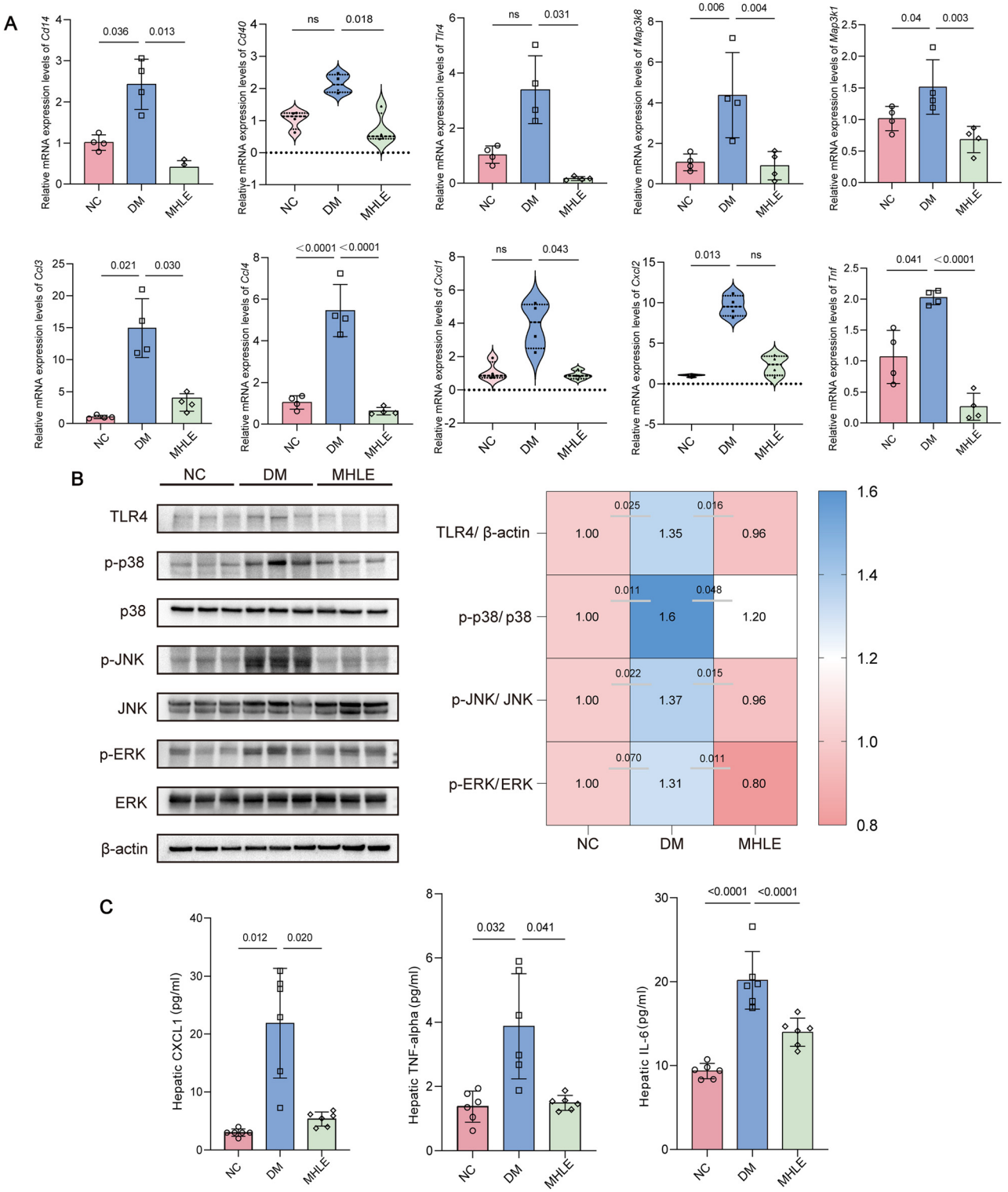

Fig. 6 Effects of MHLE intervention on the TLR4/MAPK signaling pathway in mice liver. (A) Relative mRNA expression levels of *CD14*, *CD40*, *TLR4*, *MAP3K8*, *Map3k1*, *CCL3*, *CCL4*, *CXCL1*, *CXCL2*, And *TNF* in the liver (n = 4 biological replicates). (B) Protein expression of TLR4, p-p38, p38, p-JNK, JNK, p-ERK, and ERK in the liver (n = 3 biological replicates). (C) Hepatic CXCL1, TNF-α, and IL-6 expression measured by electrochemilumine scence (n = 6 biological replicates).

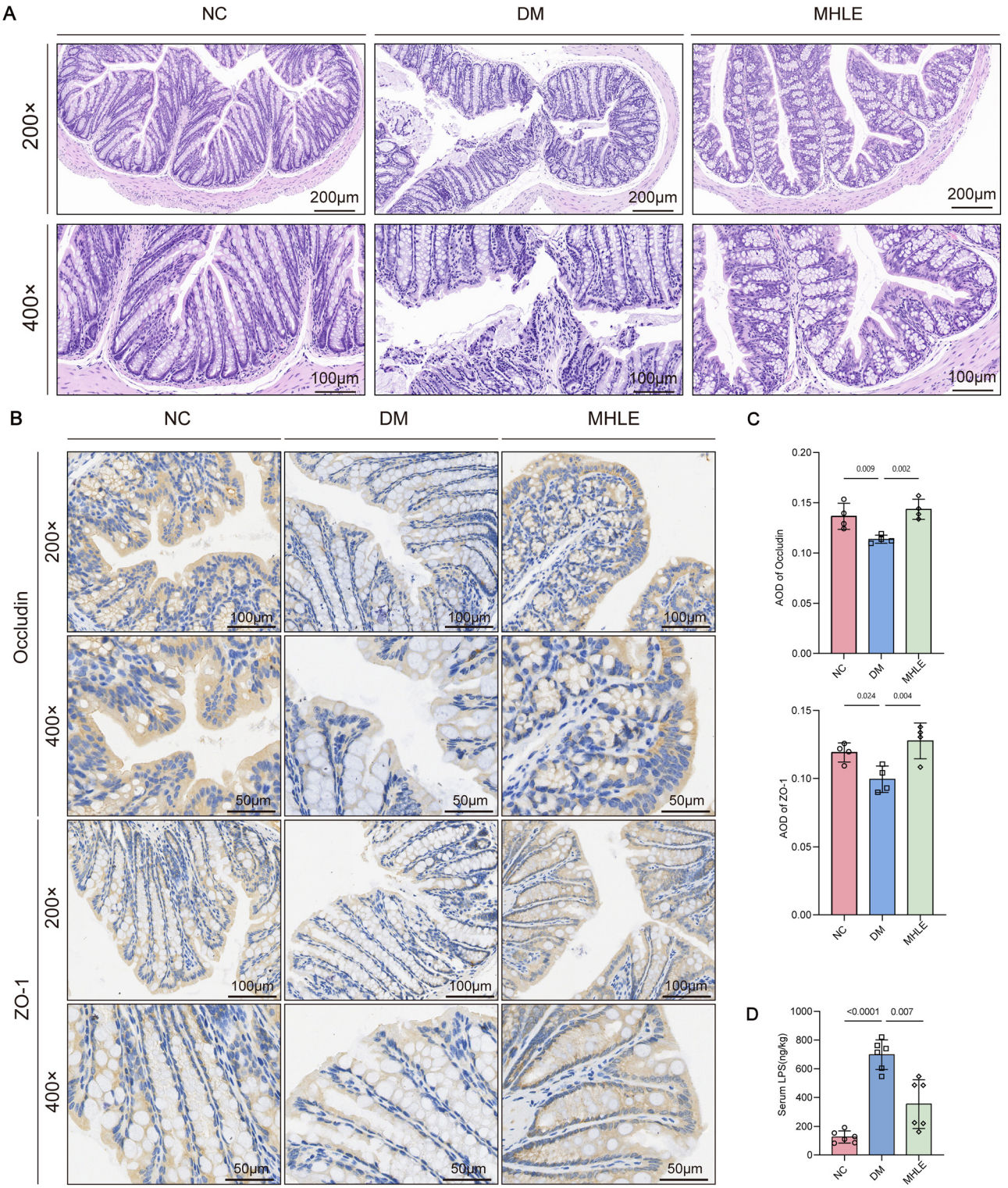

Fig. 7 MHLE improves colon barrier dysfunction in db/db mice. (A) HE staining for pathologic diagnosis of mice colons at 200× magnification (scale bars: 200 μm) and 400× magnification (scale bars: 100 μm). (B) IHC staining of ZO-1 and Occludin in mice colons at 200× magnification (scale bars: 50 μm) and 100× magnification (scale bars: 100 μm). (C) Quantitative analysis of ZO-1 and Occludin (n = 4 biological replicates). (D) Serum LPS levels (n = 6 biological replicates).

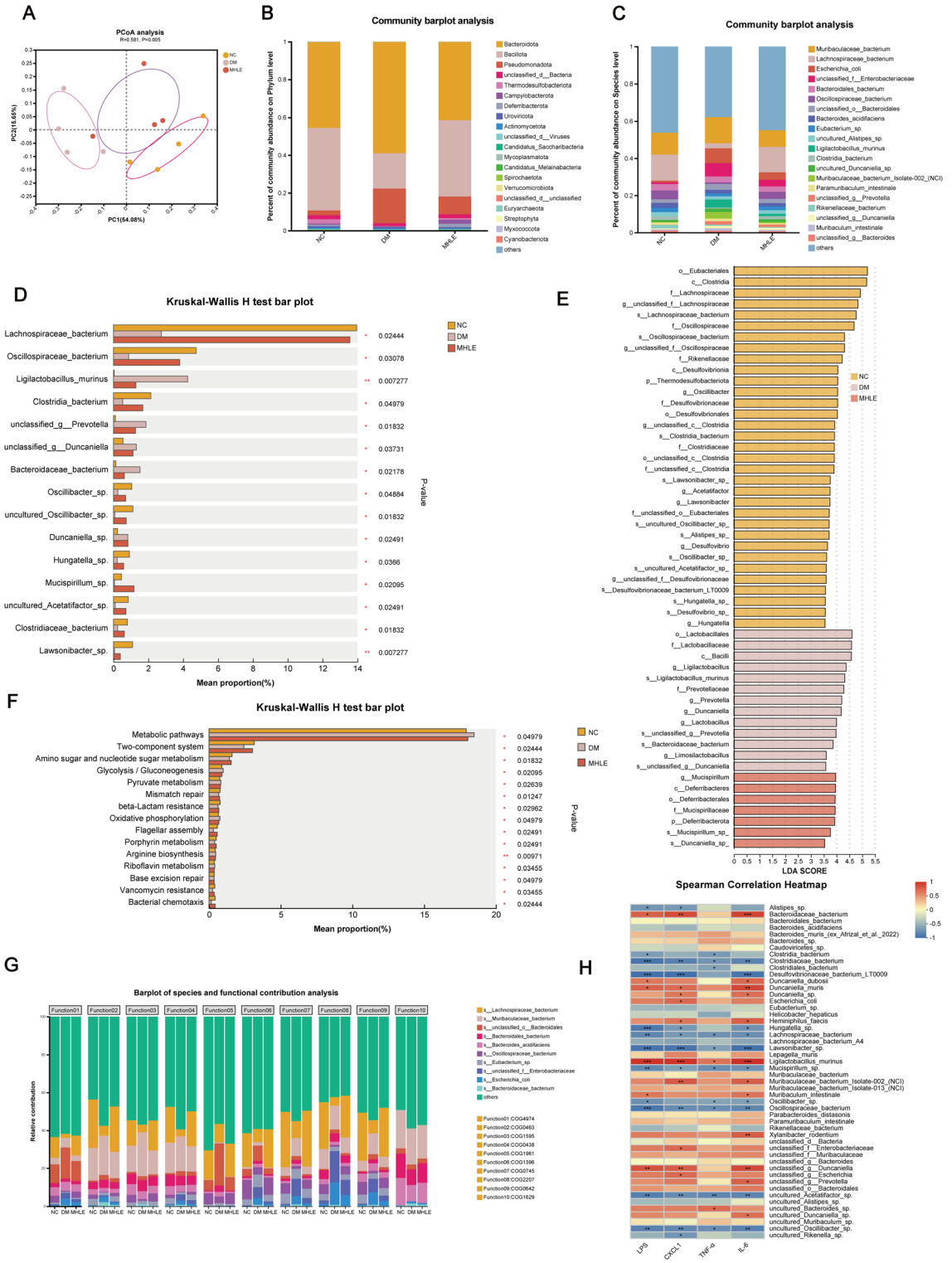

Fig. 8 MHLE reverses microbial dysbiosis. (A) Beta diversity of gut microbiota estimated by PCoA analysis at the species level. (B and C) Bar plot of microbiota community composition at the phylum and species level. (D) Comparative analysis of species levels between different groups using the Kruskal–Wallis H test. (E) LEfSe analysis from phylum to species level (LDA > 3.5, $P < 0.05$). (F) Comparative analysis of KEGG pathways (level 3) between different groups using the Kruskal–Wallis H test. (G) Correlation analysis between species and function relative abundance at the species level. (H) Correlation analysis of gut microbiota and inflammatory mediators ($n = 4$ biological replicates) *$P < 0.05$, **$P < 0.01$.

shown in Fig. 8F. Oral administration of MHLE can effectively restore pathways changes. To determine which gut microbiota contribute to the regulation of KEGG pathways, we performed an association analysis between the relative abundance of species and functions. Fig. 8G shows the top ten KEGG pathways enriched at the pathway level 3. At the species level, *Lachnospiraceae bacterium*, *Muribaculaceae bacterium*, and *Escherichia coli* are major contributors to these functions.

Correlation analysis of gut microbiota and inflammatory chemokines in db/db mice

The correlation Heatmap (Fig. 8H) visually showed the degree of correlation between 4 kinds of inflammatory chemokines and different strains, and whether the correlation difference is significant. *Lachnospiraceae bacterium*, *Mucispirillum*, *Clostridia bacterium*, *Oscillospiraceae bacterium* and *uncultured Acetatifactor* are negatively correlated with the 4 inflammatory factors. *Bacteroidaceae bacterium*, *Duncaniella muris* and *unclassified g Duncaniella* were positively correlated with LPS, CXCL1 and IL-6. *Muribaculaceae bacterium* was positively correlated with CXCL1 and IL-6, and *Escherichia coli* was positively correlated with CXCL1. These results suggest a strong association between gut microbiota and inflammatory chemokines.

Discussion

T2DM is a chronic metabolic disease with complex pathological mechanism. Functional food has great advantages and potential in the treatment of T2DM, and may have fewer side effects. Recent studies have found that various foods or their active ingredients can improve T2DM and its complications. For example, a randomized, double-blind, and controlled clinical trial found that cinnamon can reduce plasma inflammatory factors in T2DM patients.[25] Additionally, animal studies have shown that black wheat can improve T2DM and its complications by regulating glucose transporters.[26] Fu brick tea can reshape the gut microbiota to alleviate T2DM symptoms.[27] The development of functional foods holds unlimited potential.

In this study, the chemical composition of MHLE was identified to be rich in phloretin, phloretin and other dihydrochalcones, suggesting that MHL is a promising candidate food for the prevention and treatment of T2DM. Compared with a single pharmacological study of active ingredients such as phlorizin, the innovation of this study is that concretized the source of these ingredients, and the effects of various ingredients are integrated to show in the form of a functional food, which is more conducive to people's daily life directly and conveniently enjoy the health bene fits brought by these active ingredients.

Db/db mice has been a widely used animal model of T2DM because it can better reflect the characteristics of human T2DM.[28] In this study, we found that MHLE significantly reduced FBG and GSP in db/db mice, improved abnormal glucose tolerance, and had a beneficial effect on glycemic control. However, no clear dose-dependency was observed and the optimal dose requires further investigation. In addition, the liver maintains glucose homeostasis by storing glycogen or by gluconeogenesis. In mice with normal hepatic glucose metabolism, liver glycogen is degraded and released into the circulation during fasting to maintain stable glucose levels. Conversely, in mice with liver dysfunction due to metabolic abnormalities and chronic hyperglycemia, liver glycogen accumulates. The abnormal increase in liver glycogen is considered to be one of the critical factors in uncontrolled blood glucose levels in diabetes.[29] We observed that wt/wt mice had lower hepatic glycogen stores after 12 hours of fasting compared to db/db mice, which had higher levels. This suggests that hyperglycemia in db/db mice leads to abnormal accumulation of hepatic glycogen, but oral administration of MHLE can ameliorate this condition to some extent. Dyslipidemia is also a common feature in diabetic patients, with TC, TG, HDL and LDL often serving as dyslipidemia indicators.[30] In our study, the oral administration of MHLE led to improvements in these indicators of dyslipidemia. However, we did not observe a significant weight loss effect after five weeks of treatment, which is in contrast to the weight loss observed after four weeks of MHLE administration in high-fat diet-induced obese mice.[19] This difference could be due to different genetic backgrounds, and perhaps extending the experimental duration would result in observable weight loss in db/db mice.

Disruption of the gut microbiome in T2DM can induce chronic low-grade inflammation in multiple organs.[31] Gut microbial carbohydrate metabolism can also contribute to the development of insulin resistance.[32] Fecal microbiota transplantation has been found to improve total and low-density lipoprotein cholesterol levels, as well as liver stiffness, in obese subjects with T2DM.[33] The supplementation of probiotics, prebiotics, synbiotics, and postbiotics has been shown to improve metabolic diseases,[34] and various polysaccharides and polyphenols present in food have also been demonstrated to help improve T2DM.[35,36] In this study, diabetic mice had reduced intestinal tight junction proteins (ZO-1, Occludin) and altered colon structure, which may be related to changes in the gut microbiome. Metagenomics showed that the abundance of *Lachnospiraceae bacterium*, *Oscillospiraceae bacterium*, *Clostridia bacterium* in the gut of db/db mice decreases. These are butyrate-producing bacteria from the *Bacillota* phylum. Butyrate plays a role in maintaining intestinal homeostasis and epithelial cell integrity, serving as the primary energy source for colonic cells.[37] In patients with T2DM, epithelial cell integrity is disrupted and butyrate production is reduced.[38,39] Butyrate-producing *Clostridium butyricum* can improve gut barrier function and alleviate inflammation.[40] Additionally, supplementation with *Clostridium butyricum* significantly reduces hepatic inflammation induced by carbon tetrachloride.[41] *Lachnospiraceae* is a protective commensal strain capable of producing butyrate and other short-chain fatty acids through the fermentation of dietary fiber.[42] A longitudinal human cohort study conducted in China[43] using gut shotgun metagenomics found that the *Lachnospiraceae bacter-*

ium 3 1 57FAA CT1 was negatively correlated with HOMA-IR. The abundance of the *Lachnospiraceae bacterium 28-4* in the mice gut microbiota is negatively correlated with host metabolic health parameters.[44] In addition, *Oscillospira* is considered one of the candidates for next-generation probiotics.[45]

Loss of beneficial bacteria is a pathogenic factor, on the other hand, the acquisition of pathogens is also associated with disease. In diabetic mice, we observed an increase in the abundance of *Escherichia coli* and *unclassified Enterobacteriaceae*. *Escherichia coli* is a bacterium within the family *Enterobacteriaceae*, belonging to the phylum *Pseudomonadota*. *Enterobacteriaceae* bacteria can cause dysfunction in the gut mucosal immune system, leading to damage to the gut barrier and the onset of chronic systemic inflammation.[46] An increased abundance of commensal *Escherichia coli* is a common phenomenon in patients with metabolic imbalance and individuals with excessive weight gain.[47] *Escherichia coli* colonization significantly increases obesity, impairs glucose tolerance, and leads to increased inflammation in liver, adipose, and intestinal tissues in mice fed a high-fat diet.[48] It has been reported that 14 probiotic strains isolated from fermented camel milk can reduce *Escherichia coli* and LPS, and improve glucose and lipid metabolism disorders in db/db mice.[49] In this study, MHLE intervention significantly promoted the proliferation of the above beneficial bacteria, while inhibiting the growth of harmful bacteria, which may be part of the reason why MHLE alleviated tissue inflammation and improved glucose and lipid metabolism.

Mitigating inflammatory damage in T2DM is a major focus of both basic and clinical research. The liver, a critical target organ for insulin, is also an important immune organ. With the concept of gut-liver axis proposed, researchers have paid more attention to the relationship between intestinal microbiota imbalance and hepatic inflammation. The portal vein is the signature anatomical structure of gut–liver communication, liver receive intestine-derived blood through the portal vein,[50] which makes the liver more susceptible to gut bacteria, bacterial products, endotoxins, and inflammatory mediators. Especially when the intestinal immune barrier is damaged, on the one hand, the bacteria in it can directly shift to the liver along with the blood to cause inflammation, on the other hand, gut-derived endotoxins such as LPS can also enter the portal vein circulation, producing inflammatory mediators and cytokines, and aggravating the damage to the liver.[51] Macrophages respond to signals from the tissue microenvironment by undergoing classical M1 pro-inflammatory or alternative M2 anti-inflammatory activation. Inflammatory macrophages have been implicated in reducing insulin sensitivity in the liver, skeletal muscle, and pancreatic β-cell cells.[52] There are two major populations of macrophages in the liver: Kupffer cells (KCs) and monocyte-derived macrophages. Macrophages respond to signals from the tissue microenvironment by undergoing classical M1 pro-inflammatory or alternative M2 anti-inflammatory activation. In particular, inflammatory macrophages have been implicated in reducing insulin sensitivity in the liver, skeletal muscle, and pancreatic β-cell cells.[52] KCs reside in the hepatic sinusoids, are typically exposed to bacteria, microbial debris, and endotoxins of intestinal origin. KCs are highly sensitive to gut-derived endotoxins, particularly LPS. We found a significant increase in serum LPS in db/db mice, which may be caused by the gut microbiome disturbance mentioned above, and the correlation analysis results supported this conjecture. LPS, a major component of the outer membrane of Gram-negative bacteria, has been consistently recognized as a key factor in triggering this inflammatory response.[53] When LPS binds to surface receptors on KCs, it activates intracellular signaling pathways, including toll-like receptors 2 and TLR4, nuclear factor-κB, ERK1, p38, and JNK. Activation of these pathways induces KCs to release a variety of pro-inflammatory cytokines such as TNF-α, IL-1β, IL-6, IL-12, and IL-18, and chemokines such as CXCL1-3, CXCL8, and CCL2 to CCL4, which may contribute to hepatocyte dysfunction.[54,55]

In addition, pro-inflammatory cytokines and lipids derived from visceral obesity are factors that activate pro-inflammatory pathways in KCs.[52] Under conditions of obesity, KCs are activated into an M1 state where they attract inflammatory monocytes to migrate into the liver and promote the differentiation of these monocytes into monocyte-derived macrophages.[56] This process results in a significant increase in the proportion of macrophages in the liver, exacerbating hepatic inflammation and insulin resistance. Similarly, our research results show that compared to the control group, diabetic mice exhibit diffuse hepatocellular steatosis and a significant increase in the number of hepatic F4/80 macrophages and CD86-labeled M1 phenotype, as well as a notable increase in hepatic inflammatory factors IL-6, TNF-α and chemokine CXCL1, and MHLE treatment significantly attenuated these changes. Our subsequent RNA-seq analysis suggested that MHLE may exert hepatoprotective effects against T2DM by regulating inflammatory pathways such as TLR4/MAPK. Molecular biological techniques confirmed that MHLE not only obstructs the transcription of LPS-mediated related receptor genes upstream of TLR4, but also inhibits the transmission of a variety of downstream MAPK signals including ERK, JNK, and p38 by reducing protein phosphorylation. These findings suggest that the anti-inflammatory effect of MHLE on the liver of T2DM may be based on the inhibition of M1 polarization of hepatic macrophages and the conduction of related inflammatory signaling pathways. Before our study, several foods and their main components had already been reported to have anti-inflammatory effects and the potential to combat T2DM. Recent studies have shown[57] that using a high-fat diet and a streptozotocin-induced rat model combined with LPS-treated bone marrow-derived macrophages, *Grifola frondosa* polysaccharide intervention improves metabolic disorders in T2DM, alleviates hepatic inflammation, and exerts anti-inflammatory effects by inhibiting M1 macrophage polarization and promoting M2 polarization. Additionally, *Lycopene*[58] regulates the inflammation of pancreatic islets to alleviate hyperglycemia. Pomegranate peel polyphenols significantly reduce plasma

levels of IL-6, TNF-α, and high-sensitivity C-reactive protein in T2DM patients.[59] Our study further confirms the effectiveness of anti-inflammatory therapy as a strategy for T2DM treatment and demonstrates the broad potential of functional foods in the fields of anti-inflammation and anti-diabetes.

Limitation

This study has confirmed that MHL, functioning as a healthful food, exhibits a significant improvement in glycolipid metabolism, intestinal flora, and hepatic inflammation in diabetic db/db mice, with short-term administration deemed safe. However, due to the lack of identified dose-effect relationship in this research, the optimal intake for humans remains undetermined. Similarly, the long-term effects on humans necessitate further evaluation through controlled clinical trials. While the main chemical components of MHLE have been analyzed using UHPLC-QE-MS, other potentially active ingredients have yet to be fully identified. Therefore, the core components and their mechanisms, which play a pivotal role in MHLE, require further exploration.

Conclusions

This study demonstrates that MHLE effectively alleviates T2DM symptoms through multiple mechanisms, including improved glucose and lipid metabolism, reduced hepatic inflammation, and modulation of gut microbiota composition in db/db mice. The effects of MHLE on the gut-liver axis are particularly significant, as modulation of gut microbiota composition leads to a reduction in gut dysbiosis and a decrease in inflammatory signals transmitted to the liver. By downregulating the TLR/MAPK pathway, MHLE suppresses hepatic inflammatory responses and helps restore metabolic and immune balance across the gut-liver axis. These findings underscore the potential of MHL as a functional food ingredient with antidiabetic properties and support its integration into dietary strategies for the management of T2DM. If further validation is achieved in the context of clinical trials, MHL has the potential to become a valuable component of strategies aimed at addressing the global diabetes epidemic. Its incorporation into dietary guidelines and functional food products could offer a cost-effective and sustainable approach to improving metabolic health and potentially preventing T2DM-related complications.

Author contributions

Q. Zhang: conceptualization, writing – original draft, writing – review and editing, data curation. T. Su: writing – original draft, writing – review and editing, formal analysis, software. Y. Pan: writing – original draft, validation, visualization. X. Wang: formal analysis, investigation. C. Zhang: methodology, formal analysis, investigation. H. Qin: methodology, formal analysis. M. Li: software, formal analysis. Q. Li: investigation, formal analysis. X. Li: investigation, formal analysis. J. Guo: investigation, formal analysis. L. Wu: investigation, validation, resources. L. Qin: visualization, supervision, resources. T. Liu: project administration, funding acquisition, data curation.

Ethical approval

All animal experimental procedures were conducted in accordance with the National Institutes of Health Guide for the Care and Use of Laboratory Animals and were approved by the Animal Care and Ethics Committee of Beijing University of Traditional Chinese Medicine (No. BUCM-2023091906-3197, Approval date: Oct. 12, 2023).

Data availability

Sequencing data for this study can be found in online repositories.

Transcriptomics: **https://dataview.ncbi.nlm.nih.gov/object/PRJNA1143730?reviewer=lhv6rj231uj9onkfpov5be5suc**

Metagenomics: **https://dataview.ncbi.nlm.nih.gov/object/PRJNA1143890?reviewer=ias0d3t1kb5kg273p3opstcafo**

Conflicts of interest

There are no conflicts to declare.

Acknowledgements

This work was supported by the Creation and Talent Introduction Base of Prevention and Treatment of Diabetes and Its Complications with Traditional Chinese Medicine (No. B20055).

References

1 E. Ahmad, S. Lim, R. Lamptey, D. R. Webb and M. J. Davies, Type 2 diabetes, *Lancet*, 2022, **400**, 1803–1820.
2 H. Sun, P. Saeedi, S. Karuranga, M. Pinkepank, K. Ogurtsova, B. B. Duncan, C. Stein, A. Basit, J. C. N. Chan, J. C. Mbanya, M. E. Pavkov, A. Ramachandaran, S. H. Wild, S. James, W. H. Herman, P. Zhang, C. Bommer, S. Kuo, E. J. Boyko and D. J. Magliano, IDF diabetes atlas: Global, regional and country-level diabetes prevalence estimates for 2021 and projections for 2045, *Diabetes Res. Clin. Pract.*, 2022, **183**, 109119.
3 M. Y. Donath and S. E. Shoelson, Type 2 diabetes as an inflammatory disease, *Nat. Rev. Immunol.*, 2011, **11**, 98–107.

4 G. Xourafa, M. Korbmacher and M. Roden, Inter-organ crosstalk during development and progression of type 2 diabetes mellitus, *Nat. Rev. Endocrinol.*, 2024, **20**, 27–49.
5 T. Houben, Y. Oligschlaeger, A. V. Bitorina, T. Hendrikx, S. M. A. Walenbergh, M.-H. Lenders, M. J. J. Gijbels, F. Verheyen, D. Lütjohann, M. H. Hofker, C. J. Binder and R. Shiri-Sverdlov, Blood-derived macrophages prone to accumulate lysosomal lipids trigger oxLDL-dependent murine hepatic inflammation, *Sci. Rep.*, 2017, **7**, 12550.
6 A. Alkhatib, C. Tsang, A. Tiss, T. Bahorun, H. Arefanian, R. Barake, A. Khadir and J. Tuomilehto, Functional foods and lifestyle approaches for diabetes prevention and management, *Nutrients*, 2017, **9**, 1310.
7 I. Medina-Vera, M. Sanchez-Tapia, L. Noriega-López, O. Granados-Portillo, M. Guevara-Cruz, A. Flores-López, A. Avila-Nava, M. L. Fernández, A. R. Tovar and N. Torres, A dietary intervention with functional foods reduces metabolic endotoxaemia and attenuates biochemical abnormalities by modifying faecal microbiota in people with type 2 diabetes, *Diabetes Metab.*, 2019, **45**, 122–131.
8 P. Li, J. Tan, M. Xiao, X. Cai, H. Xue and H. Yu, Bioactive substances and biological functions in malus hupehensis: A review, *Molecules*, 2023, **28**, 658.
9 Q. Lv, Y. Lin, Z. Tan, B. Jiang, L. Xu, H. Ren, W. C. Tai, C. Chan, C. Lee, Z. Gu, D. K. W. Mok and S. Chen, Dihydrochalcone-derived polyphenols from tea crab apple (Malus hupehensis) and their inhibitory effects on α-glucosidase in vitro, *Food Funct.*, 2019, **10**, 2881–2887.
10 Y. Cao, W. Yao, T. Yang, M. Yang, Z. Liu, H. Luo, Z. Cao, R. Chang, Z. Cui, H. Zuo and B. Liu, Elucidating the mechanisms of buyang huanwu decoction in treating chronic cerebral ischemia: A combined approach using network pharmacology, molecular docking, and in vivo validation, *Phytomedicine*, 2024, **132**, 155820.
11 S. Edirs, L. Jiang, X. Xin and H. A. Aisa, Kursi wufarikun ziyabit improves the physiological changes by regulating endoplasmic reticulum stress in the type 2 diabetes db/db mice, *Evid. Based Complement. Alternat. Med.*, 2021, **2021**, 2100128.
12 M. D. Fullerton, S. Galic, K. Marcinko, S. Sikkema, T. Pulinilkunnil, Z. Chen, H. M. O'Neill, R. J. Ford, R. Palanivel, M. O'Brien, D. G. Hardie, S. L. Macaulay, J. D. Schertzer, J. R. B. Dyck, B. J. van Denderen, B. E. Kemp and G. R. Steinberg, Single phosphorylation sites in Acc1 and Acc2 regulate lipid homeostasis and the insulin–sensitizing effects of metformin, *Nat. Med.*, 2013, **19**, 1649–1654.
13 A. B. Nair and S. Jacob, A simple practice guide for dose conversion between animals and human, *J. Basic Clin. Pharm.*, 2016, **7**, 27–31.
14 D. Guo, J. Li, Y. Shi and J. Wang, Study on the flavon ingredients of malus hupehensis, *Zhongguo Zhongyao Zazhi*, 2011, **34**, 1026–1029.
15 F. Dalgaard, N. P. Bondonno, K. Murray, C. P. Bondonno, J. R. Lewis, K. D. Croft, C. Kyrø, G. Gislason, A. Scalbert, A. Cassidy, A. Tjønneland, K. Overvad and J. M. Hodgson, Associations between habitual flavonoid intake and hospital admissions for atherosclerotic cardiovascular disease: A prospective cohort study, *Lancet Planet. Health*, 2019, **3**, e450–e459.
16 Z. Li, Q. Wen, J. Pi, D. Zhang, J. Nie, W. Wei, W. Li and D. Guo, An inulin-type fructan isolated from *Serratula chinensis* alleviated the dextran sulfate sodium-induced colitis in mice through regulation of intestinal barrier and gut microbiota, *Carbohydr. Polym.*, 2023, **320**, 121206.
17 L. W. Sumner, A. Amberg, D. Barrett, M. H. Beale, R. Beger, C. A. Daykin, T. W.-M. Fan, O. Fiehn, R. Goodacre, J. L. Griffin, T. Hankemeier, N. Hardy, J. Harnly, R. Higashi, J. Kopka, A. N. Lane, J. C. Lindon, P. Marriott, A. W. Nicholls, M. D. Reily, J. J. Thaden and M. R. Viant, Proposed minimum reporting standards for chemical analysis, *Metabolomics*, 2007, **3**, 211–221.
18 C. Wen, D. Wang, X. Li, T. Huang, C. Huang and K. Hu, Targeted isolation and identification of bioactive compounds lowering cholesterol in the crude extracts of crabapples using UPLC-DAD-MS-SPE/NMR based on pharmacology-guided PLS-DA, *J. Pharm. Biomed. Anal.*, 2018, **150**, 144–151.
19 Y. Wu, H. Sun, R. Yi, X. Liao, J. Li, H. Li, F. Tan and X. Zhao, Malus hupehensis leaves extract attenuates obesity, inflammation, and dyslipidemia by modulating lipid metabolism and oxidative stress in high-fat diet-induced obese mice, *J. Food Biochem.*, 2020, **44**, e13484.
20 J. Sha, J. Song, M. Yu, X. Zhao, H. Wang, Y. Zhang and H. Suo, Polyphenolic extracts from wushan tea leaves attenuate hepatic injury in CCl4-treated mice, *J. Funct. Foods*, 2020, **66**, 103826.
21 R. Rej, Aminotransferases in disease, *Clin. Lab. Med.*, 1989, **9**, 667–687.
22 F. Wroblewski, The clinical significance of alterations in transaminase activities of serum and other body fluids, *Adv. Clin. Chem.*, 1958, **1**, 313–351.
23 K. Kashani, M. H. Rosner and M. Ostermann, Creatinine: From physiology to clinical application, *Eur. J. Intern. Med.*, 2020, **72**, 9–14.
24 L. P. Bechmann, R. A. Hannivoort, G. Gerken, G. S. Hotamisligil, M. Trauner and A. Canbay, The interaction of hepatic lipid and glucose metabolism in liver diseases, *J. Hepatol.*, 2012, **56**, 952–964.
25 M. Davari, R. Hashemi, P. Mirmiran, M. Hedayati, S. Sahranavard, S. Bahreini, R. Tavakoly and B. Talaei, Effects of cinnamon supplementation on expression of systemic inflammation factors, NF-kB and sirtuin-1 (SIRT1) in type 2 diabetes: A randomized, double blind, and controlled clinical trial, *Nutr. J.*, 2020, **19**, 1.
26 V. Tiwari, A. Kamboj, B. Sheoran, E. Chaudhary, M. Yadav, A. Kumari, M. Krishania, U. Ali, A. Tiwari, M. Garg and A. Bhatnagar, Anthocyanin-rich black wheat as a functional food for managing type 2 diabetes mellitus: A study on high fat diet-streptozotocin-induced diabetic rats, *Food Funct.*, 2025, DOI: **10.1039/D4FO05065G**.
27 X. Zhang, Q. Li, N. Han, C. Song, Y. Lin, L. Zhang, D. Ren, Y. Zhao, X. Yang and T. Li, Effects of fu brick tea polysac-

charides on gut microbiota and fecal metabolites of HFD/STZ-induced type 2 diabetes rats, *Food Funct.*, 2023, **14**, 10910–10923.

28 A. Guilbaud, M. Howsam, C. Niquet-Léridon, F. Delguste, E. Boulanger and F. J. Tessier, The LepR $^{db/db}$ mice model for studying glycation in the context of diabetes, *Diabetes Metab. Res. Rev.*, 2019, **35**, e3103.

29 M. C. Petersen, D. F. Vatner and G. I. Shulman, Regulation of hepatic glucose metabolism in health and disease, *Nat. Rev. Endocrinol.*, 2017, **13**, 572–587.

30 R. M. Krauss, Lipids and lipoproteins in patients with type 2 diabetes, *Diabetes Care*, 2004, **27**, 1496–1504.

31 R. Caesar, C. S. Reigstad, H. K. Bäckhed, C. Reinhardt, M. Ketonen, G. Östergren Lundén, P. D. Cani and F. Bäckhed, Gut-derived lipopolysaccharide augments adipose macrophage accumulation but is not essential for impaired glucose or insulin tolerance in mice, *Gut*, 2012, **61**, 1701–1707.

32 T. Takeuchi, T. Kubota, Y. Nakanishi, H. Tsugawa, W. Suda, A. T.-J. Kwon, J. Yazaki, K. Ikeda, S. Nemoto, Y. Mochizuki, T. Kitami, K. Yugi, Y. Mizuno, N. Yamamichi, T. Yamazaki, I. Takamoto, N. Kubota, T. Kadowaki, E. Arner, P. Carninci, O. Ohara, M. Arita, M. Hattori, S. Koyasu and H. Ohno, Gut microbial carbohydrate metabolism contributes to insulin resistance, *Nature*, 2023, **621**, 389–395.

33 S. C. Ng, Z. Xu, J. W. Y. Mak, K. Yang, Q. Liu, T. Zuo, W. Tang, L. Lau, R. N. Lui, S. H. Wong, Y. K. Tse, A. Y. L. Li, K. Cheung, J. Y. L. Ching, V. W. S. Wong, A. P. S. Kong, R. C. W. Ma, E. Y. K. Chow, S. K. H. Wong, I. C. H. Ho, P. K. S. Chan and F. K. L. Chan, Microbiota engraftment after faecal microbiota transplantation in obese subjects with type 2 diabetes: A 24-week, double-blind, randomised controlled trial, *Gut*, 2022, **71**, 716–723.

34 H.-Y. Li, D.-D. Zhou, R.-Y. Gan, S.-Y. Huang, C.-N. Zhao, A. Shang, X.-Y. Xu and H.-B. Li, Effects and mechanisms of probiotics, prebiotics, synbiotics, and postbiotics on metabolic diseases targeting gut microbiota: A narrative review, *Nutrients*, 2021, **13**, 3211.

35 W. Liu, Y. Zhang, M. Zheng, Y. Ye, M. Shi, X. Wang, L. Cao and L. Wang, Polysaccharides in medicinal and food homologous plants regulate intestinal flora to improve type 2 diabetes: Systematic review, *Phytomedicine*, 2024, **134**, 156027.

36 U. Shabbir, M. Rubab, E. B.-M. Daliri, R. Chelliah, A. Javed and D.-H. Oh, Curcumin, quercetin, catechins and metabolic diseases: The role of gut microbiota, *Nutrients*, 2021, **13**, 206.

37 H. M. Hamer, D. Jonkers, K. Venema, S. Vanhoutvin, F. J. Troost and R.-J. Brummer, Review article: The role of butyrate on colonic function, *Aliment. Pharmacol. Ther.*, 2008, **27**, 104–119.

38 L. Macia, A. N. Thorburn, L. C. Binge, E. Marino, K. E. Rogers, K. M. Maslowski, A. T. Vieira, J. Kranich and C. R. Mackay, Microbial influences on epithelial integrity and immune function as a basis for inflammatory diseases, *Immunol. Rev.*, 2012, **245**, 164–176.

39 J. Qin, Y. Li, Z. Cai, S. Li, J. Zhu, F. Zhang, S. Liang, W. Zhang, Y. Guan, D. Shen, Y. Peng, D. Zhang, Z. Jie, W. Wu, Y. Qin, W. Xue, J. Li, L. Han, D. Lu, P. Wu, Y. Dai, X. Sun, Z. Li, A. Tang, S. Zhong, X. Li, W. Chen, R. Xu, M. Wang, Q. Feng, M. Gong, J. Yu, Y. Zhang, M. Zhang, T. Hansen, G. Sanchez, J. Raes, G. Falony, S. Okuda, M. Almeida, E. LeChatelier, P. Renault, N. Pons, J.-M. Batto, Z. Zhang, H. Chen, R. Yang, W. Zheng, S. Li, H. Yang, J. Wang, S. D. Ehrlich, R. Nielsen, O. Pedersen, K. Kristiansen and J. Wang, A metagenome-wide association study of gut microbiota in type 2 diabetes, *Nature*, 2012, **490**, 55–60.

40 M. K. Stoeva, J. Garcia-So, N. Justice, J. Myers, S. Tyagi, M. Nemchek, P. J. McMurdie, O. Kolterman and J. Eid, Butyrate-producing human gut symbiont, Clostridium butyricum, and its role in health and disease, *Gut Microbes*, 2021, **13**, 1907272.

41 J. Liu, Y. Fu, H. Zhang, J. Wang, J. Zhu, Y. Wang, Y. Guo, G. Wang, T. Xu, M. Chu and F. Wang, The hepatoprotective effect of the probiotic Clostridium butyricum against carbon tetrachloride-induced acute liver damage in mice, *Food Funct.*, 2017, **8**, 4042–4052.

42 M. Vacca, G. Celano, F. M. Calabrese, P. Portincasa, M. Gobbetti and M. De Angelis, The controversial role of human gut lachnospiraceae, *Microorganisms*, 2020, **8**, 573.

43 K. Deng, M. Shuai, Z. Zhang, Z. Jiang, Y. Fu, L. Shen, J.-S. Zheng and Y. Chen, Temporal relationship among adiposity, gut microbiota, and insulin resistance in a longitudinal human cohort, *BMC Med.*, 2022, **20**, 171.

44 Z. Li, E. Zhou, C. Liu, H. Wicks, S. Yildiz, F. Razack, Z. Ying, S. Kooijman, D. P. Y. Koonen, M. Heijink, S. Kostidis, M. Giera, I. M. J. G. Sanders, E. J. Kuijper, W. K. Smits, K. W. Van Dijk, P. C. N. Rensen and Y. Wang, Dietary butyrate ameliorates metabolic health associated with selective proliferation of gut Lachnospiraceae bacterium 28-4, *JCI Insight*, 2023, **8**, e166655.

45 J. Yang, Y. Li, Z. Wen, W. Liu, L. Meng and H. Huang, Oscillospira - a candidate for the next-generation probiotics, *Gut Microbes*, 2021, **13**, 1987783.

46 M. Y. Zeng, N. Inohara and G. Nuñez, Mechanisms of inflammation-driven bacterial dysbiosis in the gut, *Mucosal Immunol.*, 2017, **10**, 18–26.

47 C. L. J. Karlsson, J. Önnerfält, J. Xu, G. Molin, S. Ahrné and K. Thorngren-Jerneck, The microbiota of the gut in preschool children with normal and excessive body weight, *Obesity*, 2012, **20**, 2257–2261.

48 T. Ju, B. C. T. Bourrie, A. J. Forgie, D. M. Pepin, S. Tollenaar, C. M. Sergi and B. P. Willing, The gut commensal escherichia coli aggravates high-fat-diet-induced obesity and insulin resistance in mice, *Appl. Environ. Microbiol.*, 2023, **89**, e01628–e01622.

49 Y. Wang, D. Dilidaxi, Y. Wu, J. Sailike, X. Sun and X. Nabi, Composite probiotics alleviate type 2 diabetes by regulating intestinal microbiota and inducing GLP-1 secretion in db/db mice, *Biomed. Pharmacother.*, 2020, **125**, 109914.

50 X. Yang, D. Lu, J. Zhuo, Z. Lin, M. Yang and X. Xu, The gut-liver axis in immune remodeling: New insight into liver diseases, *Int. J. Biol. Sci.*, 2020, **16**, 2357–2366.
51 H. Tilg, T. E. Adolph and M. Trauner, Gut-liver axis: Pathophysiological concepts and clinical implications, *Cell Metab.*, 2022, **34**, 1700–1718.
52 R. Meshkani and S. Vakili, Tissue resident macrophages: Key players in the pathogenesis of type 2 diabetes and its complications, *Clin. Chim. Acta*, 2016, **462**, 77–89.
53 C. R. H. Raetz and C. Whitfield, Lipopolysaccharide endotoxins, *Annu. Rev. Biochem.*, 2002, **71**, 635–700.
54 G. C. Farrell, D. van Rooyen, L. Gan and S. Chitturi, NASH is an inflammatory disorder: Pathogenic, prognostic and therapeutic implications, *Gut Liver*, 2012, **6**, 149–171.
55 R. Meli, G. Mattace Raso and A. Calignano, Role of innate immune response in non-alcoholic Fatty liver disease: metabolic complications and therapeutic tools, *Front. Immunol.*, 2014, **5**, 177.
56 A. E. Obstfeld, E. Sugaru, M. Thearle, A.-M. Francisco, C. Gayet, H. N. Ginsberg, E. V. Ables and A. W. Ferrante, C-C chemokine receptor 2 (CCR2) regulates the hepatic recruitment of myeloid cells that promote obesity-induced hepatic steatosis, *Diabetes*, 2010, **59**, 916–925.
57 P. Zou, X. Li, L. Wang, Y. She, C. Xiao, Y. Peng, X. Qian, P. Luo and S. Wei, Grifola frondosa Polysaccharide Ameliorates Inflammation by Regulating Macrophage Polarization of Liver in Type 2 Diabetes Mellitus Rats, *Mol. Nutr. Food Res.*, 2024, **68**, 2400392.
58 Y. Liu, Y. Tian, X. Dai, T. Liu, Y. Zhang, S. Wang, H. Shi, J. Yin, T. Xu, R. Zhu, Y. Zhang, D. Zhao, S. Gao, X.-D. Wang, L. Wang and D. Zhang, Lycopene ameliorates islet function and down-regulates the TLR4/MyD88/NF-κB pathway in diabetic mice and Min6 cells, *Food Funct.*, 2023, **14**, 5090–5104.
59 M. Grabež, R. Škrbić, M. P. Stojiljković, V. Vučić, V. R. Grujić, V. Jakovljević, D. M. Djuric, R. Suručić, K. Šavikin, D. Bigović and N. Vasiljević, A prospective, randomized, double-blind, placebo-controlled trial of polyphenols on the outcomes of inflammatory factors and oxidative stress in patients with type 2 diabetes mellitus, *Rev. Cardiovasc. Med.*, 2022, **23**, 57.

